Supplementary Materials for

Visualizing Antibody Affinity Maturation in Germinal Centers

Jeroen M.J. Tas, Luka Mesin, Giulia Pasqual, Sasha Targ, Johanne T. Jacobsen, Yasuko M. Mano, Casie S. Chen, Jean-Claude Weill, Claude-Agnès Reynaud, Edward P. Browne, Michael Meyer-Hermann, Gabriel D. Victora

Correspondence to: victora@wi.mit.edu

This PDF file includes:

Other Supplementary Materials for this manuscript includes the following:

Materials and Methods

Mice and treatments

Rosa26^{Confetti} (*16*), *Rosa26*$^{lox\text{-}stop\text{-}lox\text{-}tdTomato}$ (Ai9 strain) (*34*), Mx1-Cre (*35*), MD4 (HEL-specific BCR-transgenic) (*36*), B6.SJL (CD45.1), B6/129 F1, and BALB/c mice (for Friend Virus passaging) were obtained from Jackson Laboratories. *Aicda*^{Cre} (*20*), B1-8^{hi} (*37*), and Photoactivatable (PA)-GFP-transgenic (*9*) mice were bred and maintained in our laboratory. *Aicda*^{CreERT2} mice (*22*) were a kind gift from Claude-Agnès Reynaud and Jean-Claude Weill (Institut Necker). All mice were bred and maintained in specific pathogen-free (SPF) or enhanced-barrier facilities at the Whitehead Institute for Biomedical Research. In our animal facility, approximately 90% of lymphocytes in Mx1-Confetti mice recombine Brainbow alleles spontaneously during early life, regardless of whether they are bred and housed in SPF housing or in an enhanced barrier facility for severely immunocompromised strains (data not shown). To generate GCs, mice were immunized in the footpad with 10 μg of chicken gamma globulin (Rockland Immunochemicals), chicken ovalbumin (OVA) (Sigma, Cat#A5503), NP-OVA (Biosearch Tech.), or recombinant influenza hemagglutinin (H3 Wisconsin/67/05), produced in S2 drosophila cells as described (*38*), a kind gift from A. Schmidt and S. Harrison (Harvard Medical School). Proteins were precipitated in 1/3 volume of Imject Alum (ThermoScientific). Recombination of the *Rosa26*^{Confetti} allele in *Aicda*^{CreERT2} mice was induced by a single gavage of 15 mg of tamoxifen (Sigma, Cat# T5648) dissolved in corn oil at 30 mg/ml. For *in vivo*-labeling of FDC networks, mice were injected intravenously with 10 μg of non-blocking monoclonal antibody (clone 8C12, kindly provided by M. Carroll, Harvard Medical School) conjugated to either Alexa 488 or Alexa 633, 24 hours prior to sacrifice. All animal procedures were approved by the Committee for Animal Care of the Massachusetts Institute of Technology.

Adoptive cell transfer

Total B cells were isolated from splenocyte preparations by negative selection using anti-CD43-coupled magnetic beads (Miltenyi Biotec). For B1-8^{hi} experiments, percentage of Igλ^+ B cells was measured by flow cytometry, and a preparation of total B cells containing ~1-2 x 10^4 Igλ^+ B cells was adoptively transferred into host mice 24 h prior to immunization. To avoid rejection of donor cells due to incomplete backcrossing of *Rosa26*^{Confetti} to the C57BL6 background, B6/129S F1 mice were used as recipients. For MD4 reconstitution experiments, 2-3 x 10^7 B cells from B6.SJL (CD45.1) donors were transferred into MD4 recipients 24 h prior to immunization. For anatomical definition of GC DZs, total splenocytes were surface-labeled with 2 μM Alexa633-NHS ester (Molecular Probes/ThermoFisher cat.# A-20005) prior to B cell purification. Labeling was performed for 15 min in PBS at 37^{o}C. 2-3 x 10^7 labeled B cells from WT donors were transferred into Mx1-Confetti recipients 24 h prior to sacrifice.

Friend virus infection

FV is a retroviral complex consisting of a replication-competent virus (Friend murine leukemia virus – F-MuLV) and a replication-incompetent spleen focus-forming virus (SFFV). FV causes persistent infection in mouse erythro-lymphoid cells (*26*). Whereas susceptible (e.g., BALB/c) mouse strains succumb to erythroid leukemia,

disease remains subclinical in resistant strains (e.g., C57BL6), despite viral loads being detectable up to at least 80 days post-infection (DPI) (*39, 40*). LDV-free B-tropic Friend virus (SFFV+FMuLV) stock was a kind gift from K. Hasenkrug (NIAID). Stocks of FV for experimental infection were prepared by generating a 10% spleen homogenate from infected BALB/c mice at 10 days post-infection. The concentration of infectious units was determined by a focus-forming assay as described (*41*). For the experiments presented in this manuscript, *Rosa26*$^{Confetti/Confetti}$.*Aicda*$^{CreERT2/+}$ mice were infected intravenously with ~10^4 FFU of Friend Virus.

Mutiphoton imaging and photoactivation

LNs were harvested at different times post-immunization/infection. Adipose tissue was carefully removed under a dissecting microscope, and the LN was placed in lactated Ringer's solution between two coverslips held together with vacuum grease, as described (*42*). For Mx1-Confetti quantification, FDCs and the mantle zone were labeled by intravenous injection of Alexa 633-labeled antibody to CD35 and Alexa 633 surface-labeled naïve B cells, respectively, both 24 hours prior to imaging. Due to the strong scattering of light by fluorescent proteins, LNs from Mx1-Confetti mice could not typically be imaged whole, and were instead embedded in 4% low-melt agarose—NuSieve GTG (Lonza), heated to boiling and then cooled to 37 ^oC prior to embedding—and cut into 200 μm slices using a Leica VT1000A vibratome. Slices were then held between coverslips for imaging, as above. For Friend Virus experiments, spleens were harvested at 30 days post-infection and cut into cross-sectional slices using a double-edged razor blade and mounted as above. All imaging was performed on an Olympus FV1000 upright microscope fitted with a 25X 1.05NA Plan water-immersion objective and a Mai-Tai DeepSee Ti-Sapphire laser (Spectraphysics). Imaging of Confetti alleles was performed using λ = 930 nm excitation. Fluorescence emission was collected in three channels, using the following filter sets: a pair of CFP (480/40 nm) and YFP (525/50 nm) filters, separated by a 505 nm dichroic mirror, for CFP/GFP/YFP detection, and a third filter (605/70 nm) for RFP detection. Alexa 633-conjugated antibody and surface-labeled naïve B cells were imaged using 810 nm excitation and a 665/40 nm emission filter. For intravital imaging, mice were anesthetized with 1-2% isoflurane in O_2. Hind legs were shaved, mice were placed on a stage heated to 37^oC, and a small incision was made behind the hind knee joint to expose the popliteal lymph node (LN), as described previously (*9*). Single-colored GCs were identified by scanning and a single Z-plane was imaged repeatedly for ~15 min using the settings detailed above.

For early GC photoactivation experiments (day 6 post-immunization), we labeled follicular dendritic cell (FDC) networks by intravenous injection of anti-CD35 antibody conjugated to Alexa 488, 24 hours prior to imaging. Photoactivation was performed as described (*9*). Briefly, clusters of tdTomato$^+$ cells within Alexa 488-positive FDC networks were identified by imaging at λ = 940 nm, at which no photoactivation is observed, and 3D regions of interest were photoactivated at λ = 830 nm. For late GC photoactivation experiments (day 15 post-immunization), FDC networks were labeled by intraperitoneal injection of 20 μg of rabbit polyclonal anti-B-PE antibody (Rockland) followed by footpad injection of 10 μg B-PE (Molecular Probes/ThermoFisher), as described (*43*).

Image analysis

Color dominance in Mx1-Confetti mice was quantified on a single Z-plane. The GC dark zone (DZ) was identified based on Alexa 633 fluorescence (λ = 810 nm excitation) from FDC networks and transferred surface-labeled naïve B cells. The DZ was defined as an area (i) showing weak FDC staining and adjacent in either the X/Y or Z axes to an area of stronger FDC staining (corresponding to the light zone); (ii) devoid of transferred Alexa 633^+ cells; and (iii) containing at least one discernible tingible body macrophage (detected by Alexa 633 fluorescence and/or autofluorescence). Cells in the DZ area thus delimited were assigned colors using a second, independently acquired image displaying the Confetti colors (λ = 930 nm excitation). Rare GCs in which the density of colored cells was < ~70% were considered as containing an expanded unrecombined clone and were excluded from the analysis.

To follow the evolution of color dominance in AID-Confetti mice, 3D LN images were reconstructed using Bitplane Imaris software. Cells of each color/combination were counted manually in 3 2D slices, 20-30 μm apart. To obtain the normalized dominance score (NDS) for AID-Confetti GCs, we first estimated the fraction of recombined cells in multiphoton microscopy images by calculating the density of fluorescent cells per area unit (100 μm^2) within each GC. Density was calculated in areas in which cell distribution was homogeneous, and which corresponded anatomically to the GC DZ. Conveniently, the NDS for control GCs in which all GC B cells are labeled (*Aicda*$^{Cre/+}$.*Rosa26*$^{lox\text{-}stop\text{-}lox\text{-}tdTomato}$) was found to be very close to 1 (mean NDS = 1.006; see fig. S5D). Therefore, NDS can be interpreted as approximately the fraction of all B cells in a GC that carry the dominant color combination. Using this system, the mean cell density of GCs 7 days after tamoxifen treatment was 0.41 cells μm^2 (or 41% recombined cells), close to the 47% observed by flow cytometry at the same time point in a different set of mice (fig. S5A-B).

To estimate the magnitude of changes in clonal distribution among slow-evolving GCs, we generated a "divergence index" that describes small deviations from the baseline color distribution considering all colors (unlike the NDS, which considers the dominant color only). This index was computed as the sum of the absolute differences in percentage points between the observed proportions of each of the 10 colors in a given GC (% color * GC density) and the expected proportions in the absence of selection (detailed in Table S1; see fig. S5E for an illustration). Results were divided by 100.

Sample processing for flow cytometry and cell sorting

Photoactivated LNs were cut into two fragments using a #10 disposable scalpel (Miltex) under a Leica MZFLIII fluorescence stereomicroscope fitted with a PlanAPO 1.0 X objective, as described (*44*). LNs or fragments were placed in microcentrifuge tubes containing 100 μl of PBS supplemented with 0.5% BSA and 1mM EDTA (PBE), macerated using disposable micropestles (Axygen), and further dissociated into single-cell suspensions by gentle vortexing. 100 μl of 2X antibody stain (antibodies to CD38, IgD, FAS, B220, TCRβ supplemented with Fc block, see Table S2) was added to the cell suspension, which was incubated on ice for 30 min. Single cells were sorted into 96-well plates, as described below, using a FACS Aria II cell sorter.

To sort B cells from Confetti GCs, we first imaged intact LNs, as described above, to determine the orientation of GCs. LNs were then embedded in low-melt agarose and vibratome sliced as detailed above (in *Multiphoton Imaging and Photoactivation*). Slices were imaged a second time to determine GC positions. If more than one Confetti$^+$ GC was present, slices were further dissected into fragments containing a single GC using a scalpel under a dissecting stereomicroscope. Slice fragments were processed as above and stained with antibodies to B220, TCRβ, FAS, and CD38. For cell sorting, fluorescent colors were detected using the following channels: (i) 405 nm excitation, 525/50 emission (detects CFP and spillover from CFP); (ii) 488 nm excitation, 530/30 nm emission (detects GFP and YFP); (iii) 488nm excitation, 580/14 nm emission (detects YFP and RFP and limited spillover from GFP); and (iv) 561 excitation, 580/14 emission (detects RFP only). Fluorescent colors were compensated against the dyes used for antibody staining, but not against each other. The sorting gate itself was drawn using channels i and iii, relying on the spillover from GFP into those two channels to sort that population (see fig. S8). Precise assignment of colors from index-sorted cells was done post-acquisition on Diva software, v. 8.0.1, using all four channels. Further analysis of flow cytometry data for presentation was carried out using FlowJo software, v. 8.7.

Single-cell *Igh* and *Igk* PCR and sequence analysis

Sorted single cells were lysed in a guanidine thiocyanate buffer (Qiagen) supplemented with 1% β-mercaptoethanol. Nucleic acids were isolated by SPRI bead cleanup as described (*45*). RNA was reverse-transcribed into cDNA using an oligo(dT) primer and *Igh*, *Igk*, and *Igl* transcripts were amplified from cDNA by PCR as described previously (*46*). *Igh* and *Igk* PCR products were sequenced by dye-terminator (Sanger) sequencing using the C-region PCR primer for *Igh* and the V-region PCR primer for *Igk*. Antibodies produced recombinantly were sequenced in both directions. Igκ/Igλ light chain assignments in NP-specific GCs (fig. S3) were done by PCR only. Rare clones expressing both mRNA chains simultaneously were considered as Igλ$^+$. When 50% or more cells within a clone (defined by *Igh* sequence) expressed a given light chain isotype (the others having yielded no PCR product), all cells in that clone were assigned that isotype. No discrepancies in which different cells from the same *Igh* clone expressed different light chain isotypes were detected.

Ig heavy and light variable (V), diversity (D) and joining (J) gene segments were assigned using the IMGT (*47*) and VBASE2 (*48*) databases. Sequence and alignment data are presented in Database S1. In case of discrepancy between V segment assignments from the two databases, the assignment leading to the lowest number of somatic mutations was chosen. Functional V(D)J sequences were grouped into to clones only when sharing *Ighv* and *Ighj* gene segments and junction regions (identical length and more than 70% amino acid identity in CDR3). Draft clonal lineage trees were constructed using ClustalW, defining the germline sequence as the out-group. Manual editing and curation of clonal trees to correct discrepancies or phylogenetic ambiguities (e.g., reversions or shared independent mutations) was performed so as to minimize the number of branching points and mutation events.

Antibody cloning, production, and affinity measurements

Ig variable region rearrangements were cloned into F_{ab} expression vectors containing the human *IGG1* or *IGK* constant regions, modified from (*46*). Soluble His-tagged F_{ab}s were produced by transient transfection of Freestyle 293-F suspension cells (Life Technologies). In brief, cells were transfected at a density of 1×10^6/ml in Freestyle293 expression media (Gibco) using polyethylenimine-mediated DNA delivery in OptiPro SFM media (Gibco), as described in (*49*). Supernatants were collected seven days after transfection and F_{ab}s were purified by immobilized metal ion affinity chromatography using Ni Sepharose excel resin (GE Healthcare), following the manufacturer's instructions. Protein purity was assessed by SDS-PAGE and concentrations were measured by spectrophotometry.

ELISA was performed by coating 96-well ELISA plates (Costar) with 5 μg/ml of either CGG or purified IgY (Gallus Immunotech), the major component of CGG, overnight at 4 °C, then blocked with PBS 2%BSA for 2h at RT followed by 1 h RT incubation with the purified F_{ab}s, diluted in PBS 1%BSA/0.05%Tween20 from 1 μM to 10 pM. Anti-Human IgG (F_{ab} specific)−HRP antibody (Sigma) was used for detection, and assays were developed using HRP chromogenic substrate (Sigma), according to the manufacturer's instructions.

Bio-layer interferometry (BLI) was performed on an Octet RED96 instrument (ForteBio) to determine F_{ab} binding affinities. Association was measured by immersing streptavidin biosensors preloaded with biotinylated IgY (2 nM) in wells containing F_{ab}s (160 nM to 5 nM in PBS 0.1%BSA/0.02%Tween20) for 600 s. Dissociation was monitored after transfer of the biosensors into PBS 0.1%BSA/0.02%Tween20 for 900 s. K_D values were determined with a global fit 1:1 binding algorithm using the Octet data analysis software (ForteBio). All full X^2 and R^2 values provided by the Octet algorithms indicated adequate goodness of fit for all F_{ab}s tested, with the exception of F_{ab} 1.4U, the affinity of which was too low to fit globally. This F_{ab} was therefore fitted using the average of values obtained by partial and local fitting.

Statistical analysis of clonal diversity

To provide a rough estimate of the total number of clones in a GC based on a small sample, we used the bias-corrected *Chao1* formula (*21*). This is a non-parametric estimator widely used in studies of species richness in natural ecosystems. The rationale is that if many species (or clones) are detected only once, there is likely a large number of clones that have not yet been detected; when all clones have been detected at least twice, it is unlikely that new undetected clones exist. The bias-corrected *Chao1* estimate was calculated as:

$$S_{Chao1} = S_{obs} + [n/(n-1)]*[(f_1-1)^2/2(f_2+1)]$$

Where S_{obs} is the total number of species (clones) detected, f_1 is the number of clones detected exactly once, and f_2 is the number of clones detected exactly twice (*21*). The *ACE* estimator is an alternative to *Chao1* that includes into the computation all species detected up to 10 times, and is shown for completeness (*21*).

The *Chao1* estimator provides an asymptotic extrapolation of the lower bound of the total number of distinct clones in an infinitely large GC (*50*). However, these estimates are expected to rapidly plateau, so that the asymptotic extrapolation becomes a good approximation of diversity at finite GC sizes. The minimum GC size for which the Chao1 estimate is valid can be determined using formula (9), from reference (*51*). These calculations, when applied to the 8 CGG GCs presented in Figure 2, show that the estimated number of clones for a given GC size reaches 95% of the asymptotic estimate at total GC populations of ~150-630 cells (fig. S11A), short of the one thousand or more cells estimated to be present in the average early GC. [For example, a spherical GC measuring 150 μm in diameter (a typical size for day 6 post-immunization GCs, see Fig. 2A), would contain up to 1,767 cells at a density of 1 cell per 10 μm^3, compatible with our own 2D estimates (see above).] Our estimations therefore likely represent good approximations of the lower bound of clonal diversity in early GCs.

To compare the *Chao1* and *ACE* estimates for different antigens, we used rarefaction to normalize our dataset to the number of sequences obtained from the lowest-sampled GC (34, for CGG, pLN2, GC1). Thus, if a single GC yielded 50 sequences, we generated 100 random subsamples of 34 sequences from these 50, and the normalized score was the mean score for these 100 subsamples. This normalization ensures that GCs are comparable to each other regardless of the number of sequences obtained for each GC (*21*). *Chao1* (with 95% confidence intervals) and *ACE* estimations, as well as rarefaction analysis, were carried out using the EstimateS software package (http://purl.oclc.org/estimates).

Accuracy of clonal estimation using the Confetti system.

To inform our interpretation of the biological meaning of color frequencies in the Confetti system, we simulated the random recombination of *Rosa26*^{Confetti} alleles computationally. In the *in vivo* Mx1-Confetti experiment, colors are selected prior to immunization. Therefore, all cells of a given clone will have the same color, but because the number of colors is limited, multiple clones can carry the same color. We used the clonal distribution data obtained from day 15 GCs by photoactivation (Fig. 1G and fig. S2) as a basis for simulations aimed at estimating the color dominance levels produced by randomly assigning clones to colors. For each of the 12 photoactivated GCs, we carried out 25 simulations. In each simulation, clones were randomly assigned to one of the 10 color combinations (or to the non-recombined category), according to the proportions listed in Table S1, which roughly represent the probabilities observed *in vivo*. Color dominance was defined as the number of cells of the most abundant color, regardless of clonal origin. As with our experimental data, GCs with more than 30% non-recombined cells were excluded from this analysis. As shown in Figure 11B, color dominance somewhat overestimates clonal dominance, as expected given the possibility of coincidences in color choice between clones. However, this effect tends to become smaller as clonal dominance increases. Accordingly, the largest discrepancy between color and clonal distributions determined in experiment (compare Figs. 1E and 1G) is a rightward skewing of the distribution of GCs below 50% dominance.

For the AID-Confetti system, what we wish to estimate is the size of the largest "lineage" (defined as the descendants of a cell present at the time of tamoxifen-triggered recombination). Because the true lineage distribution cannot be obtained from photoactivation data (which only provides information at the clone level), we generated a set of 1,000 simulated GC distributions using a previously published agent-based model of GC selection (*52, 53*). This simulation, which originally consisted of only 3 founder clones per GC, was expanded to allow for continuous entry of clones over the first four days of the reaction (i.e. day 3-7 post-immunization). This generated clonal distributions comparable to those detected by photoactivation/sequencing presented in Figures 1, 2, S2 and S3, but for which the entire history of each cell in the final ensemble could be traced, serving as a benchmark against which we could compare color-based estimations done on the same dataset. For this, *in silico* cells were made to randomly select a color combination (or to remain non-recombined) at the equivalent of day 5 post-immunization. Color choice probability (Table S1) was defined based on experimental data from days 3-11 post-tamoxifen of the AID-Confetti-B1-8 dataset presented in Fig. 3 (which is subject to only minimal distortion by GC selection) and assuming a fraction of cells undergoing recombination of 40% (estimated from the mean colored cell density obtained in AID-Confetti GCs 7 days post-tamoxifen). Each cell present at day 5 post-immunization was considered to be a founder cell for an independent lineage. The fraction of cells belonging to the most expanded lineage at day 11 post-coloring (day 16 post-immunization) is the true degree of dominance that we wish to estimate using the Confetti system.

As seen in figure S11C, we find that the product of color dominance and the fraction of recombined cells (the *in silico* equivalent of the NDS) provides a reasonably accurate estimate of the size of the largest lineage in the GC ($r^2 = 0.78$), as long as GCs in which less than 40% of recombined cells—likely to be dominated by unrecombined lineages—are excluded from analysis. Distributions of lineage dominance in simulated GCs included or excluded from analysis based on percentage of recombined cells were indistinguishable (fig. S11D). Therefore, the color distributions obtained in the AID-Confetti experiment after exclusion of GCs dominated by unrecombined cells are likely representative of lineage dominance in all GCs.

Other statistical analysis:

Columns in Fig. 2D were compared using the nonparametric Kruskall-Wallis test followed by the Dunn's multiple comparison post-test. Columns in Fig. 3F. were compared in pairs (AID-Confetti vs. AID-Confetti-B1-8) for each time point, using the nonparametric Mann-Whitney U test. In Fig. 3G, day 3 and day 15 time points were compared within each experimental system, and day 15 timepoints between genotypes, also using the nonparametric Mann-Whitney U test. All statistical comparisons were carried out using Graphpad Prism V. 6.0.

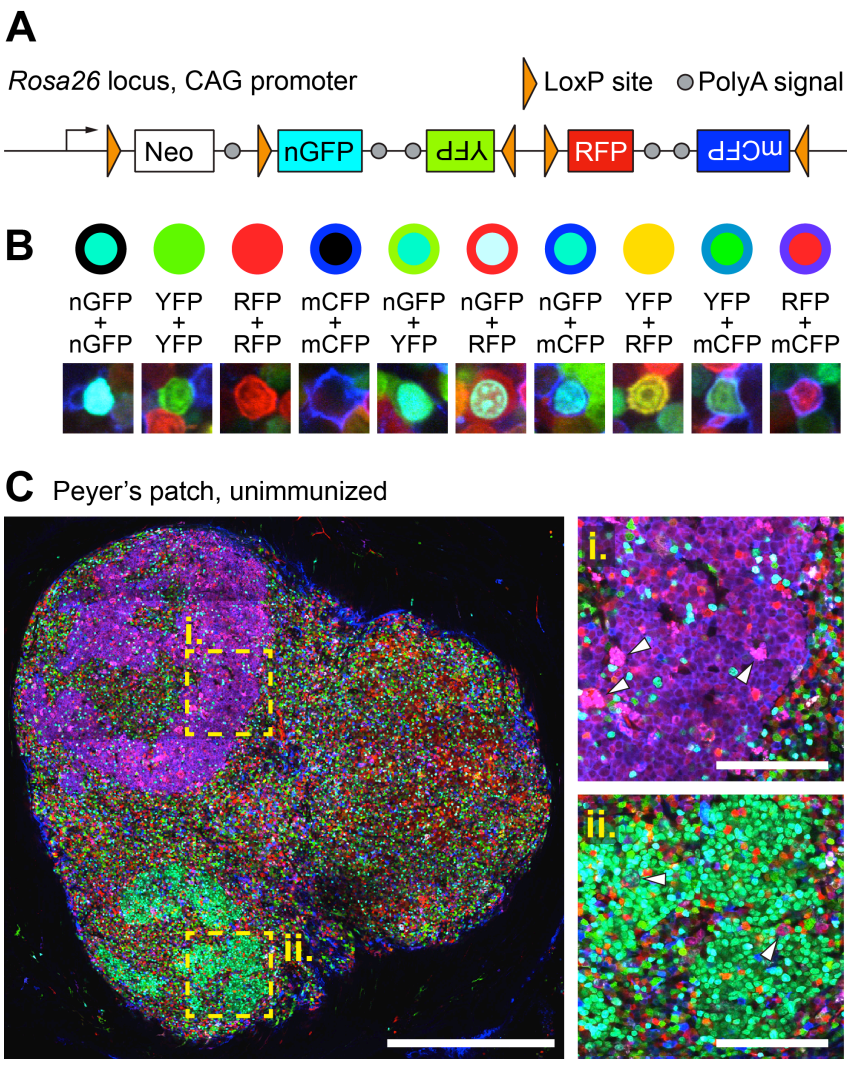

Fig. S1. Estimating clonal diversity in GCs using Confetti alleles. (**A**) Schematic representation of the *Rosa26*^{Confetti} allele, according to Snippert et al (*16*). nGFP, nuclear GFP; mCFP, membrane CFP. (**B**) Ten color combinations distinguishable by multiphoton microscopy are possible following recombination of two *Rosa26*^{Confetti} alleles in homozygous mice. Cartoon represents lymphocytes with nucleus (inner circle) and cytoplasm/membrane (outline) colored according to the expression of the fluorescent proteins indicated. Matching multiphoton images from Mx1-Confetti mice are shown below. (**C**) Unimmunized Peyer's patch from an Mx1-Confetti mouse, showing two predominantly single-colored GCs. Scale bars, 500 µm (large panel), 100 µm (side panels). Cell colors as in (B). Second harmonic generation from collagen fibers is shown in blue.

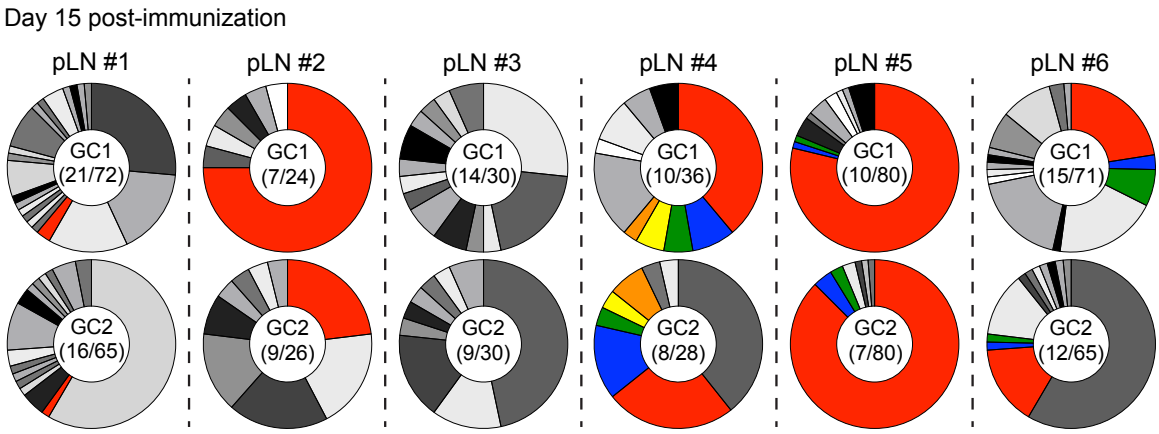

Fig. S2. Measuring clonal diversity by photoactivation. PA-GFP-transgenic mice were immunized with CGG-alum and draining pLNs were harvested 15 days later. Two individual GCs per pLN were photoactivated and separately sorted, as described in Fig. 1F. Pie charts show clonal distribution of sequenced *Igh* genes in each GC. Each slice represents one distinct clone. Colored (non-gray) slices indicate clones that were found in both GCs (upper and lower pie charts) from the same pLN. Numbers in the center of each chart are (number of clones observed/total number of cells sequenced). Pairs are from 5 different mice in 3 independent experiments.

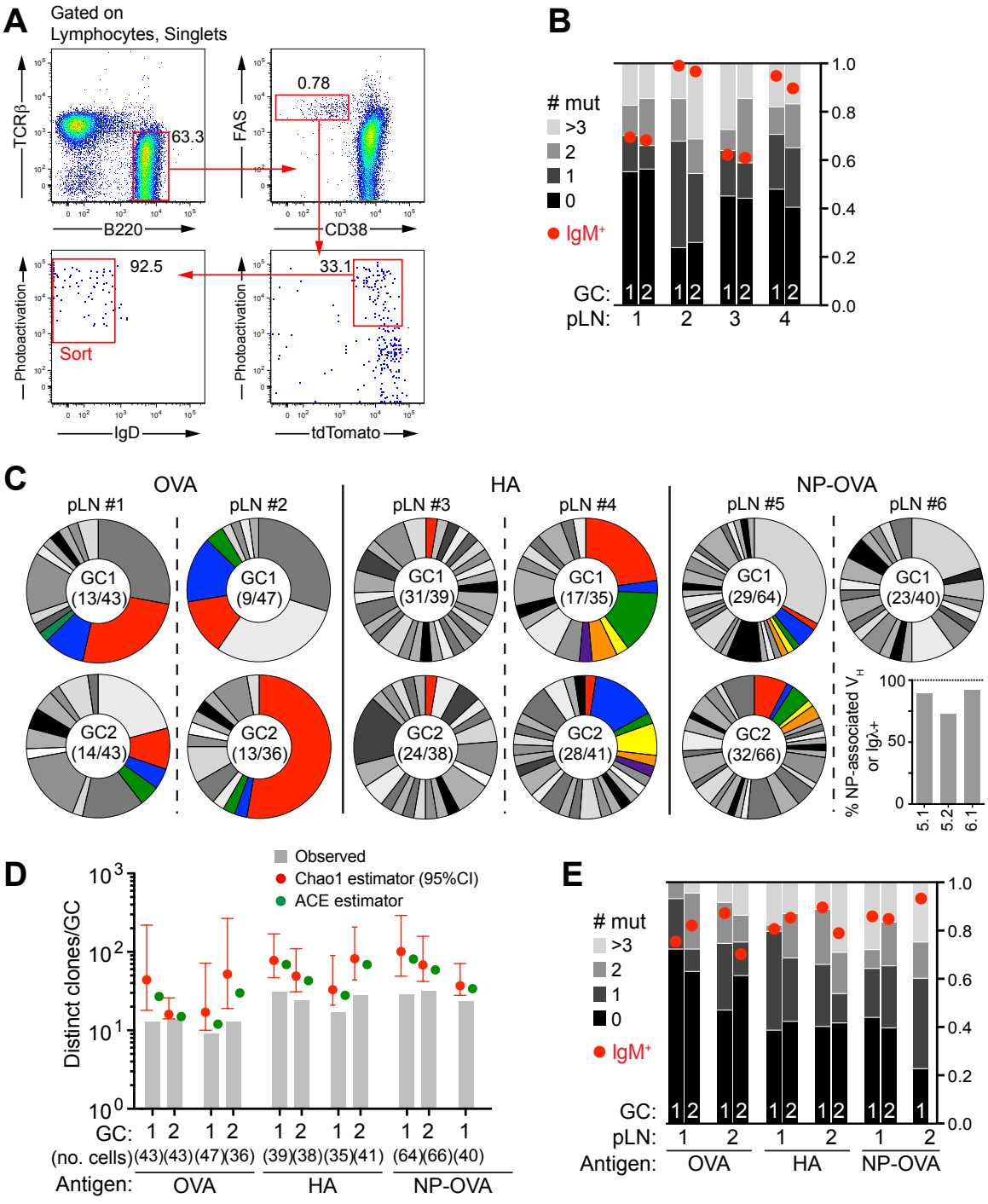

Fig. S3. Measuring clonal diversity in early GCs. PA-GFP-transgenic, Aicda$^{Cre/+}$.Rosa26$^{lox\text{-}stop\text{-}lox\text{-}tdTomato}$ mice were immunized with CGG or the indicated antigen in alum, and draining pLNs were harvested 6 days later. One or two individual GCs per pLN were photoactivated and separately sorted, as described in Fig. 2A. (**A**) Gating strategy for sorting photoactivated early GC B cells. (**B**) SHM and isotype switching in early GCs. Data corresponds to GCs shown in Fig. 2B. # mut, number of

somatic mutations in *Igh* V-segment. Grayscale bars indicate fraction of cells with the indicated number of mutations. Red circles indicate fraction of cells that have not undergone class switch recombination (IgM isotype detected in the *Igh* mRNA sequence). (**C**) Pie charts showing clonal diversity in early GCs obtained by immunization with different antigens. OVA, ovalbumin; HA, influenza hemagglutinin H3/Wisc/67/05; NP-OVA, 4-hydroxy-3-nitro-phenylacetyl-OVA. Each slice represents one clone. Colored slices represent clones that were found in both GCs (upper and lower pie charts) from the same pLN. Numbers in the center of each chart are (number of clones observed/total number of cells sequenced). Data for each antigen are from two mice in two independent experiments. Only one NP-OVA GC could be sequenced in experiment #2, therefore data on clone sharing is not available. *Bottom right*, graph showing the fraction of B cells in each GC expressing an NP-associated V_H gene [*Ighv1-72* (V186.2) (*54*), *Ighv1-64* (C1H4) (*54*), *Ighv1-53* (V23) (*54*), or *Ighv14-2* (*55*) or the closely-related *Ighv14-4*] and/or carrying an Igλ light chain. The predominance of NP-associated rearrangements provides evidence of the predominantly antigen-specific nature of the response. (**D**) Estimation of total clonal richness in individual GCs using the Chao1 and ACE estimators. Graphs show observed clonal richness (from panel (C)), and total richness according to the indicated estimator. (**E**) SHM and isotype switching in early GCs, data as in (B).

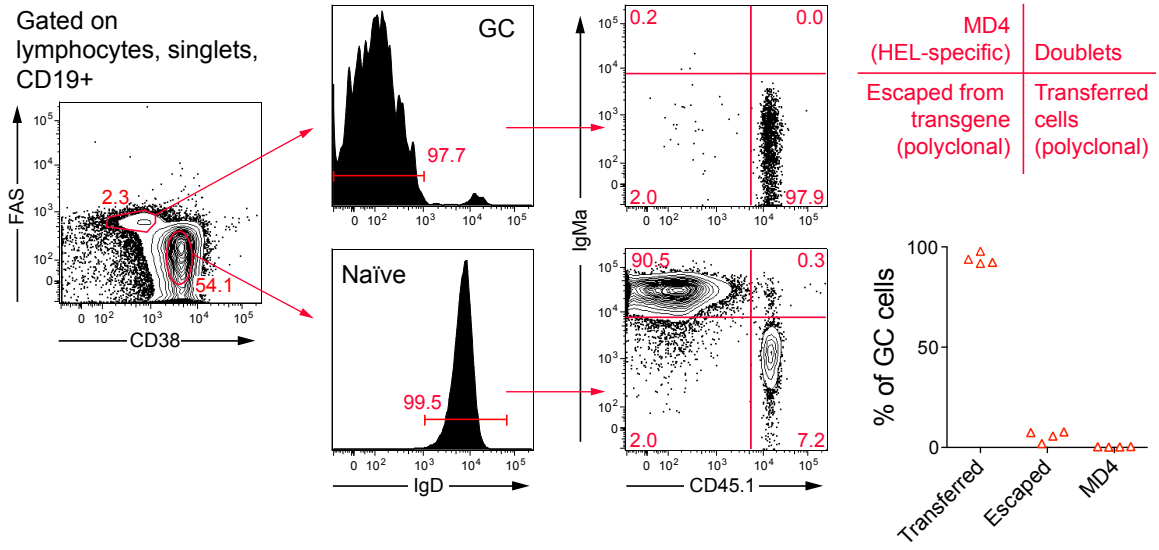

Fig. S4. B cell recruitment to early GCs is dependent on immunoglobulin specificity. To address the issue of whether all early GC B cells are antigen-specific, or whether a proportion of these cells could be recruited by non-specific polyclonal activation, we determined whether B cells with a known but irrelevant specificity would be capable of entering a GC in the presence of antigen-specific competitors. To this end, we partly reconstituted MD4 mice (in which > 95% of B cells express a transgenic IgM^a/IgD^a B cell receptor (BCR) specific for hen egg lysozyme (HEL)) with a polyclonal B cell repertoire by adoptive transfer of 2-3 x 10^7 naïve polyclonal B cells from allelically marked ($CD45.1^+$) donors. Mice were immunized 24 hours later with CGG, for which only transferred B cells or endogenous B cells that do not express the transgenic BCR (escaped cells) can be specific. pLN GCs were analyzed by flow cytometry 6 days later. *Left* and *center-left*, gating strategy for GC ($CD38^-FAS^{hi}IgD^-$) and naïve ($CD38^+FAS^{low}IgD^+$) B cell populations. *Center-right*, proportion of MD4, transgene-escaped, and transferred polyclonal cells in GCs (*top*) and among naïve B cells (*bottom*). Quadrants as defined in the *top-right* panel. *Bottom-right*, quantification of flow cytometry data for four mice from two independent experiments. Endogenous $IgMa^+$ B cells accounted for > 90% of naïve B cells in the draining LNs of reconstituted mice, but were only found in trace amounts (< 0.5%) in early GCs. Therefore, the ability of a cell to enter the early GC is dependent on the sequence of its BCR, implying that the polyclonal transferred and escaped cells that did contribute to the GC reaction were antigen-specific.

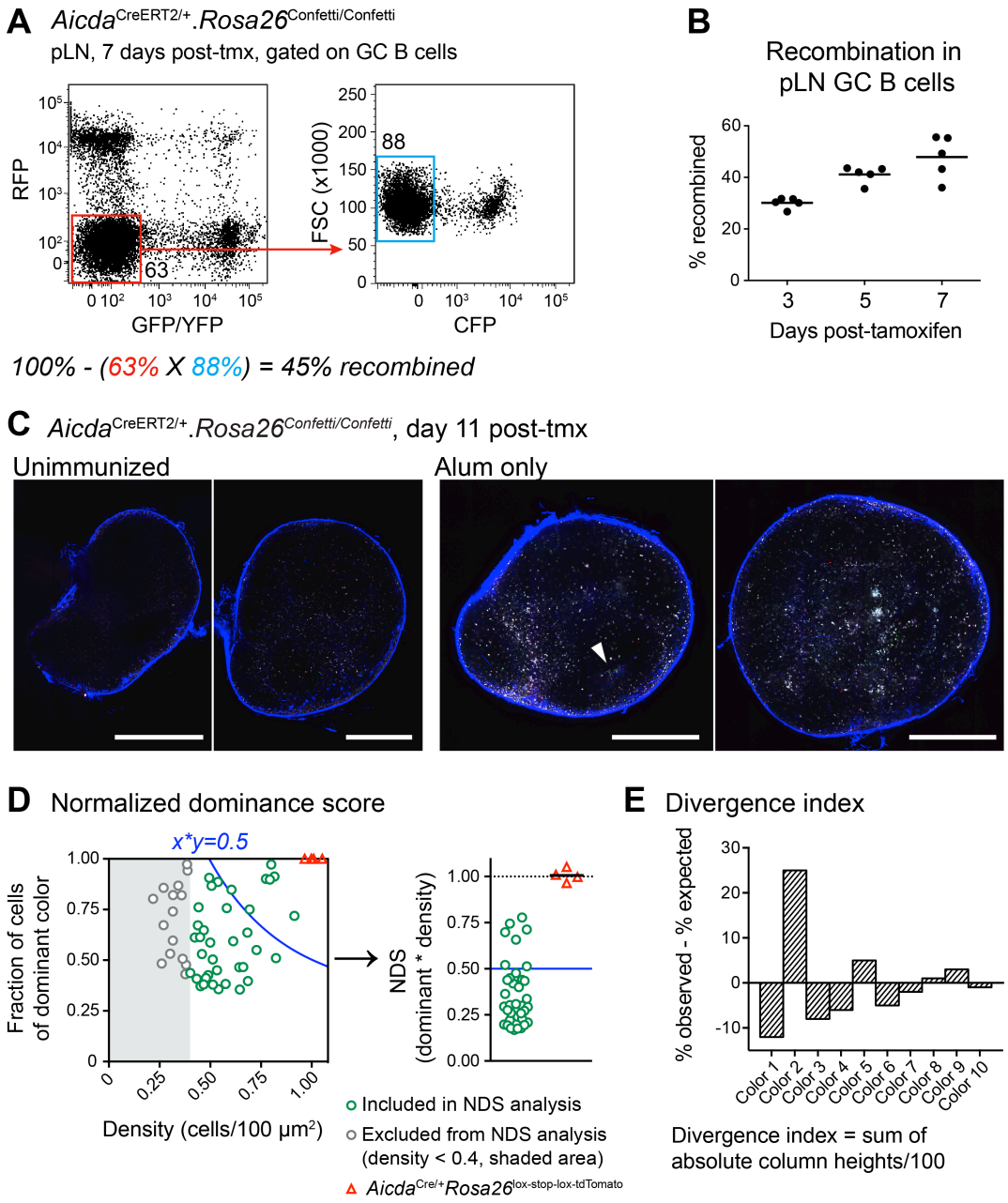

Fig. S5. Quantifying homogenizing selection using AID-Confetti mice. (**A**) Gating strategy for quantifying recombined cells. Tmx, tamoxifen. (**B**) Quantification of data as in (A). Each symbol represents one mouse. Data are pooled from two independent experiments. (**C**) GC activity in the absence of immunization. AID-Confetti mice were either left unimmunized or were injected with alum only. Mice were treated with tamoxifen 5 days later, and LNs were explanted and imaged 11 days after tamoxifen treatment. Figures show tiled multiphoton images of single Z planes of pLNs from these mice. Images are from a single experiment, and are representative of control mice included in several experiments presented in Fig. 3. A small residual GC reaction is indicated by an arrowhead. Scale bar, 500 µm. Cell colors as in fig. S1B. Second

harmonic generation from collagen fibers is shown in blue. (**D**) The normalized dominance score (NDS) was calculated by multiplying the fraction of cells of the dominant color by the density of cells in the GC DZ, in cells/100 μm^2. The graphs show this transformation for the day 11 AID-Confetti data (Fig. 3F). Each symbol corresponds to one GC. GCs with density below 0.4 cells/100 μm^2 (shaded area, gray symbols) were excluded from the analysis (see Materials and Methods). Four *Aicda*$^{Cre/+}$.*Rosa26*$^{lox\text{-}stop\text{-}lox\text{-}tdTomato}$ GCs are included for comparison (red triangles). Mean NDS for these GCs is 1.006. (**E**) The divergence index was calculated as the sum of the absolute differences in percentage points between observed proportions of each of the 10 colors and the expected proportions in the absence of selection (detailed in Table S1), represented as the absolute height of the bars in the graph. See Materials and Methods for details. Graph is illustrative, and is not based on experimental data.

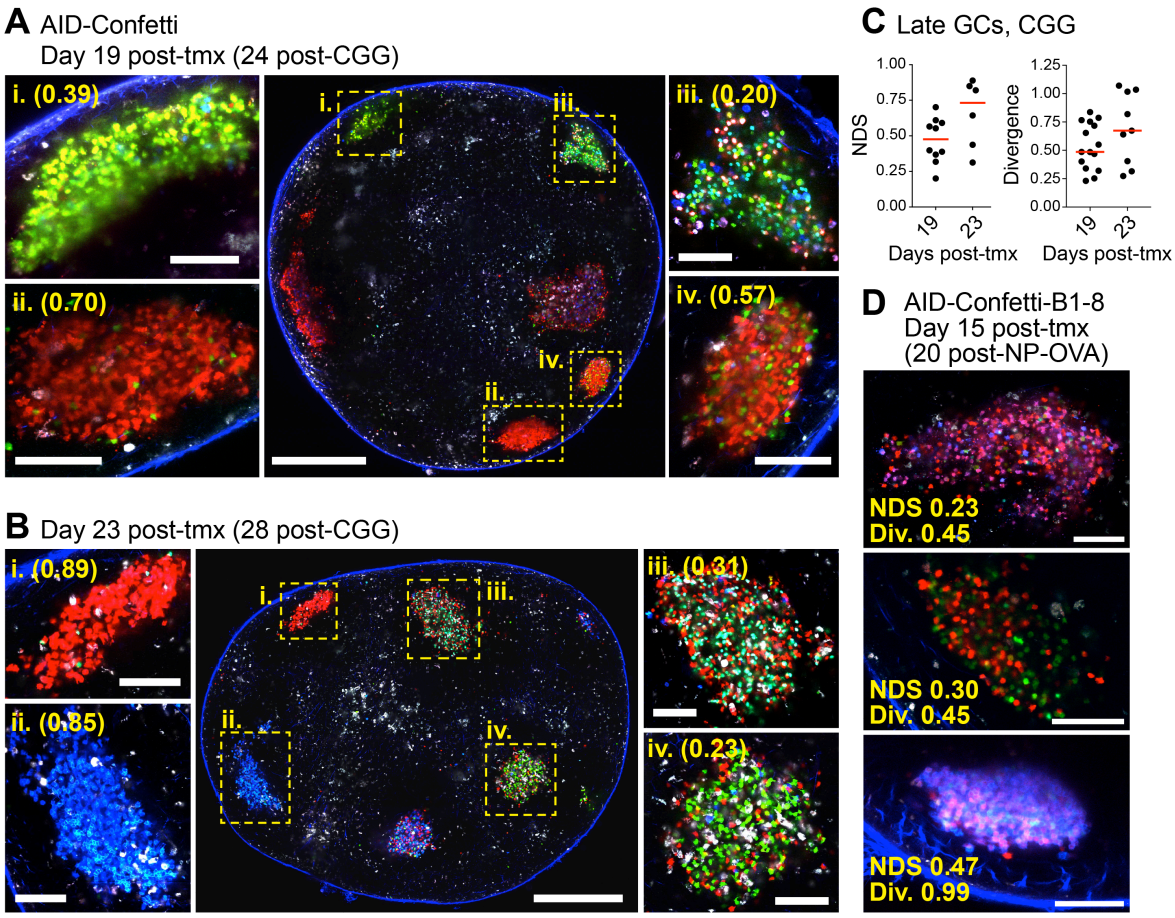

Fig. S6. Heterogeneity in color composition persists in late GCs. (**A-B**) Representative whole-LN overviews (large panel) and higher-magnification images (side panels) showing GCs at different times after tamoxifen (tmx) administration. Experimental setup as in Fig. 3A. Numbers in parentheses indicate the normalized dominance score (NDS) for each GC. Scale bar, 500 µm (overviews) and 100 µm (side panels). Side panels in (A) are from independently acquired images of the same GCs, and in (B) are higher-resolution versions of the center panel. (**C**) Quantification of data as in (A-B). Shown are NDS and divergence index. Data pooled from two mice, two experiments (day 19) and from one single mouse (day 23), representing exceptional LNs that still contained GCs at the time points imaged. Only GCs with density > 0.4 cells/µm^2 are included in the NDS analysis. (**D**) Examples of highly divergent GCs in AID-Confetti-B1-8 mice 15 days after tmx administration, as detailed in Fig. 3. Experimental setup as in Fig. 3E. Div, divergence index. Scale bars, 100 µm. Cell colors as in fig. S1B. Second harmonic generation from collagen fibers is shown in blue.

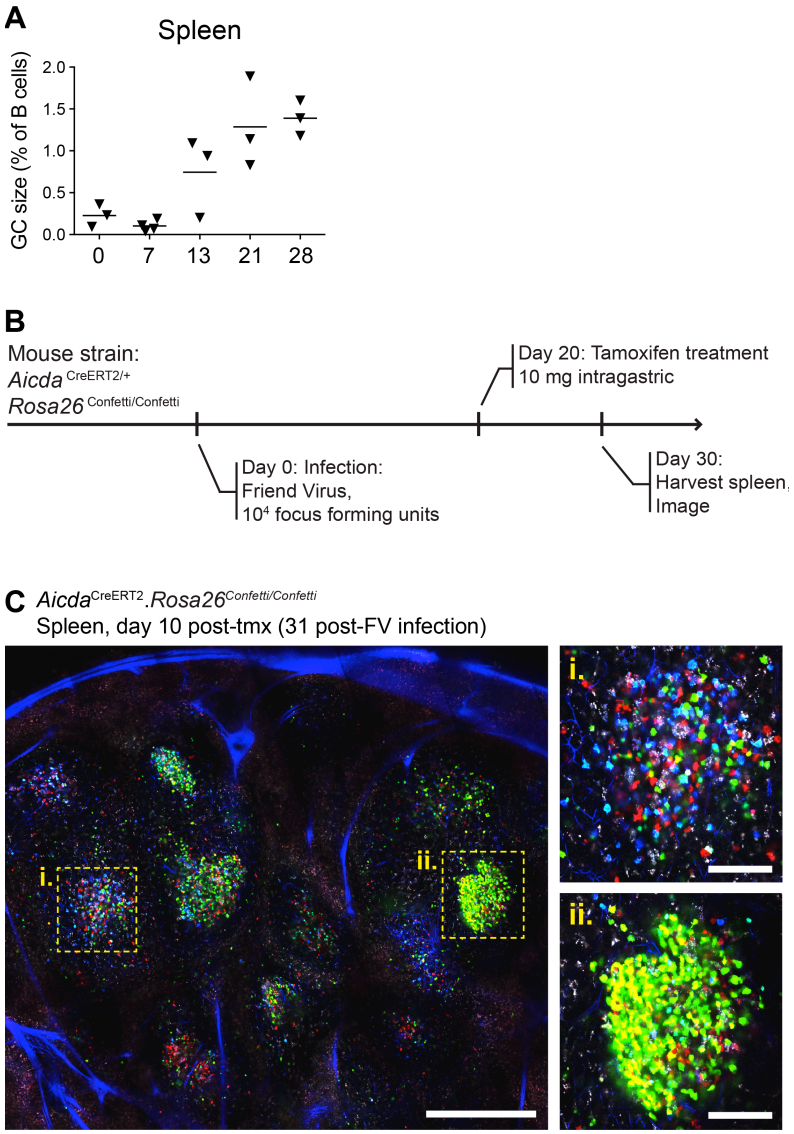

Fig. S7. GC selection during Friend Virus infection. (**A**) Kinetics of GC formation upon infection with Friend virus (FV). Mice were infected with 10^4 focus-forming units of FV at day 0 and sacrificed on the days indicated on the X-axis. Spleens were analyzed for GC content (% B cells that are $FAS^{hi}CD38^-$) by flow cytometry. Each symbol represents one mouse. Data is from a single experiment. (**B**) Experimental layout for measuring GC selection in FMLV-infected mice. (**C**) Representative image of a spleen slice 10 days after tamoxifen administration. Tiled overview (left) of a spleen slice containing multiple GCs, two of which (dashed yellow boxes) are shown in higher resolution on the right. Scale bars, 500 µm (overview), 100 µm (individual GCs). Cell colors as in fig. S1B. Second harmonic generation from collagen fibers is shown in blue.

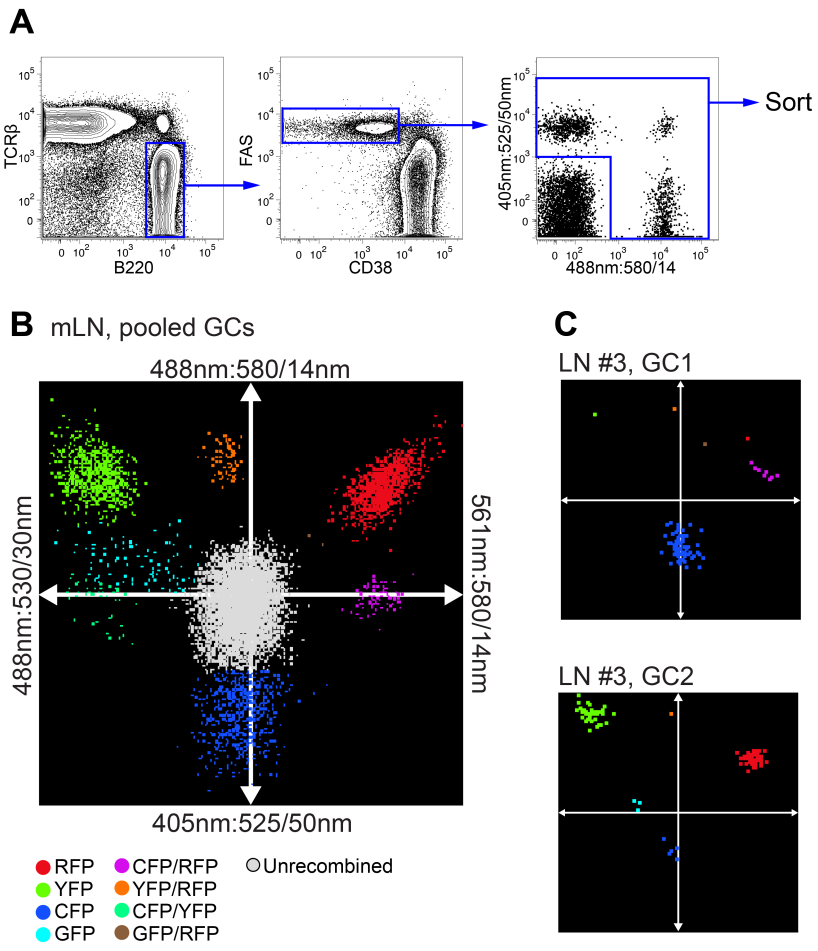

Fig. S8. Sorting strategy for *Rosa26*^{Confetti} B cells. (**A**) Strategy for sorting GC cells of all color combinations. Gating is on B cells, GC cells, and fluorescent cells, in this order. Plots from a mLN 10 days after tamoxifen administration are shown to illustrate the sorting strategy. First plot is gated on lymphocytes (forward vs. side scatter) and singlets. The right plot shows the sort gate, with axis labels indicating excitation:emission wavelengths. Further details in the Materials and Methods section. (**B**) Polyvariate plot showing mLN GC cells as in (A), oriented across the four fluorescent channels used for sorting. Axes are labeled according to excitation:emission wavelengths. (**C**) Polyvariate plots of GC cells sorted from the two pLN slices shown in fig. S9A. Axes as in (B).

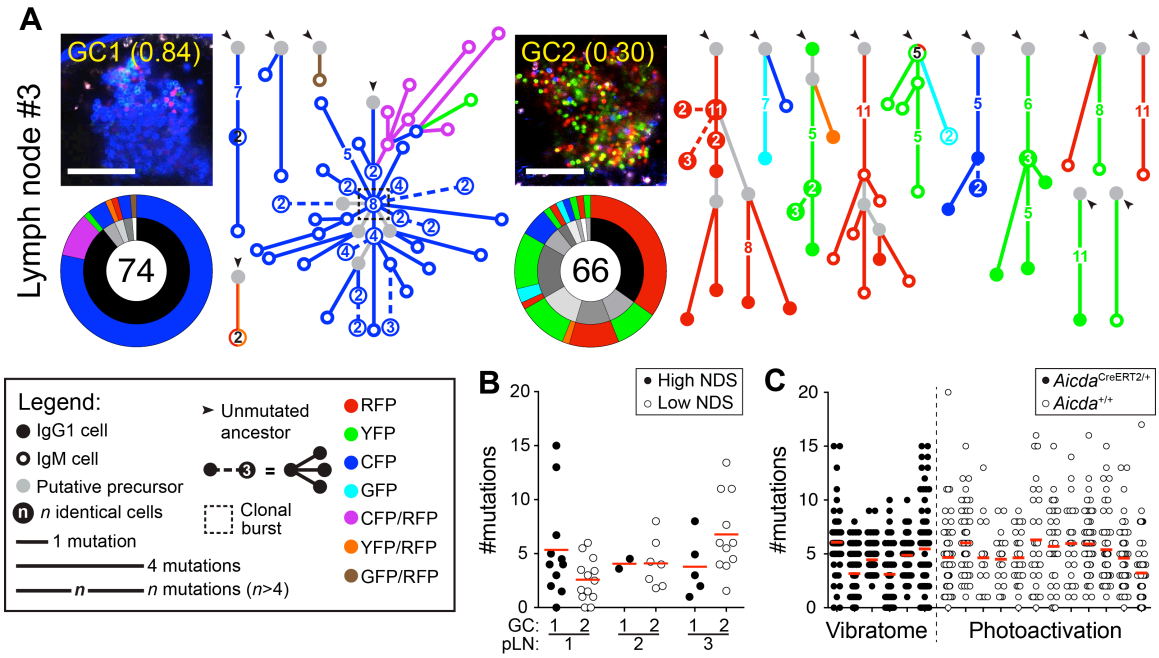

Fig. S9. Clonal relationships among cells obtained from GCs with high or low color dominance. (**A**) Sequence relationship among B cells from a pair of individual GCs from the same pLN, obtained 10 days after tamoxifen administration (15 days post-immunization). Data is from an experiment independent from those shown in Fig. 4. Each panel contains: *top left*, multiphoton image (scale bar, 100 µm, cell colors as in fig. S1B, second harmonic generation from collagen fibers is shown in blue), NDS is indicated in parentheses; *bottom left*, clonal distribution pie-chart (with clones represented in grayscale in the inner ring and Confetti colors in the outer ring; number of cells sequenced is indicated in the center); and *right*, trees representing the phylogeny of *Igh* heavy-chain V-segment sequences within each clone (symbols according to the legend in the figure). Dashed lines within the phylogenies indicate multiple different variants distanced the same number of mutations from the originating node. GC1 and GC2 were considered as displaying high and low color dominance, respectively. (**B**) Number of somatic mutations in the heavy-chain variable region in high and low-dominance GCs shown in Fig. 4B and panel (A), plotted as the mean number of mutations per clone. Each symbol represents one clone, red lines indicate mean values. Levels of SHM in high- and low-dominance GCs from the same LN did not differ systematically, indicating that differences in color dominance are not a consequence of asynchronous GC formation. (**C**) Impact of AID haploinsufficiency on SHM. Observed number of somatic mutations in *Igh* variable regions of GC B cells from *Aicda*$^{+/+}$ (empty circles) and *Aicda*$^{CreERT2/+}$ (filled circles) mice, 15 days after immunization with CGG-alum. *Aicda*$^{CreERT2/+}$ data are from GCs shown in Fig. 4 and (A); *Aicda*$^{+/+}$ data are from GCs shown in Fig. 1G and fig S2. Each symbol represents one cell, red lines indicate mean values. SHM rates in *Aicda*$^{CreERT2/+}$ cells from AID-Confetti mice were in the same range as those found in *Aicda*$^{+/+}$ cells from photoactivated GCs, indicating that absence of one functional *Aicda* allele did not substantially alter the levels of SHM in our system.

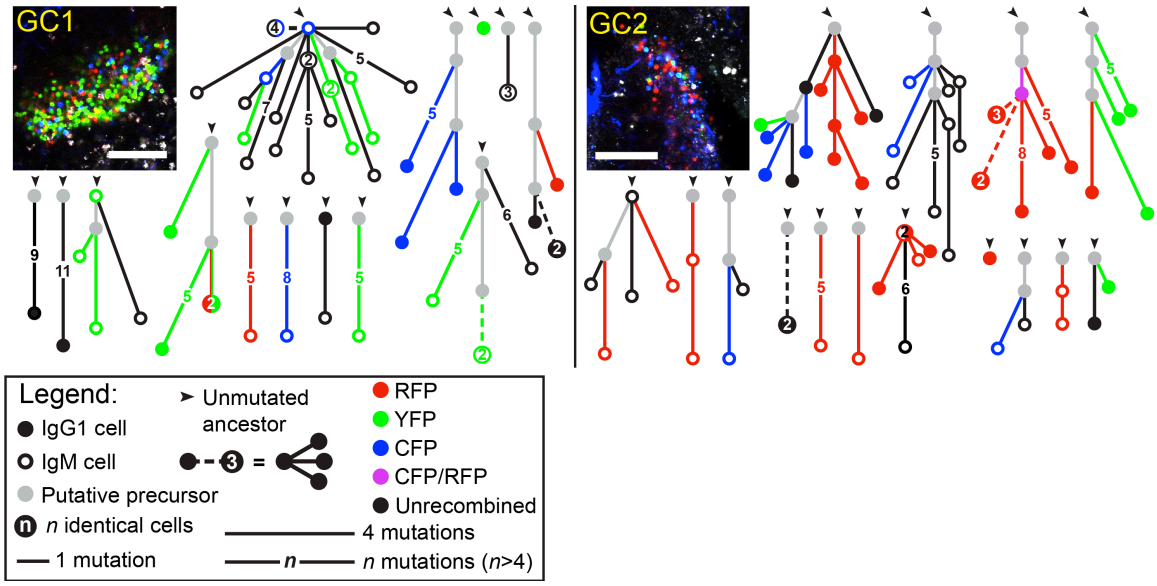

Fig. S10. Absence of large unrecombined clonal expansions from low color dominance GCs. Sequence relationships among B cells from 2 low color dominance GCs from the same pLN, obtained 10 days after tamoxifen administration (15 days post-immunization), and for which both fluorescent and nonfluorescent GC B cells were sorted. This experiment is independent from those shown in Fig. 4 and fig. S9. Each panel includes a multiphoton image of the sorted GC (scale bar, 100 μm, cell colors as in fig. S1B, second harmonic generation from collagen fibers is shown in blue) and trees representing the phylogeny of *Ig* heavy-chain V-segment sequences within each clone (symbols according to the legend below the figure). Dashed lines within phylogenies indicate multiple different variants distanced the same number of mutations from the originating node.

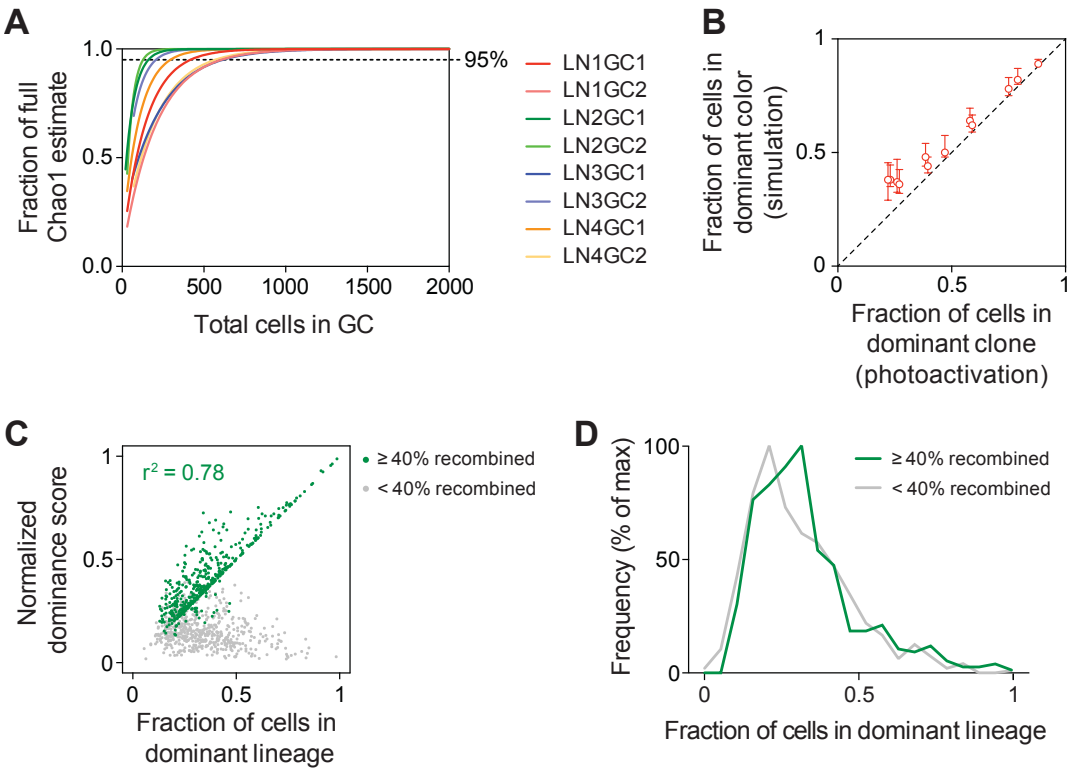

Fig. S11. Mathematical analysis. (**A**) Size dependence of Chao1 estimates of total clonality at day 6 post-immunization in photoactivated GCs. The graph shows the fraction of the full Chao1 estimate reached at different GC sizes (total number of cells). Calculations are based on the distributions of the 8 CGG-induced GCs presented in Fig. 2. Lines begin at the observed number of cells (X-axis) and clones (Y-axis) in each GC. (**B**) Accuracy of estimates using the Mx1-Confetti system. Correlation between clonal dominance in 12 photoactivated GCs (15 days post-immunization; Fig. 1G and fig. S2) and color dominance from computer-based simulations of Mx1-Confetti based on the same 12 clonal distributions. Each symbol represents the median and interquartile range of color dominances resulting from 25 simulations of the same GC. (**C-D**) Accuracy of estimates using the AID-Confetti system. (**C**) Correlation between normalized dominance score (NDS) and size of the largest lineage (as a fraction of all GC cells) in 1,000 *in silico* simulated GCs. Datasets separated by fraction of recombined cells into < 40% recombined (gray, n = 554) and ≥ 40% recombined (green, n = 446). The coefficient of determination (r^2) is given for GCs with ≥ 40% recombined cells only. (**D**) Distribution of the same 1,000 simulated GCs shown in (C) according to size of the largest lineage. See Materials and Methods for details on the mathematical analyses presented in this figure.

Table S1. Estimated proportion of cells recombining to each of the Confetti color combinations in the absence of selection.

Color combination	Proportion of cells (Mx1-Confetti)*	Proportion of cells (AID-Confetti)**
GFP/GFP or GFP/NR	5.11%	4.71%
YFP/YFP or YFP/ NR	17.20%	11.03%
RFP/RFP or RFP/ NR	17.20%	10.17%
CFP/CFP or CFP/NR	17.20%	8.81%
GFP/YFP	2.80%	0.08%
GFP/RFP	2.80%	0.27%
GFP/CFP	2.80%	0.15%
YFP/RFP	8.00%	1.18%
YFP/CFP	8.00%	1.35%
RFP/CFP	8.00%	2.27%
NR/NR	10.89%	60.00%

NR, not recombined.

* Proportions estimated based on an independent recombination probability for each Confetti allele of 20% each for CFP/YFP/RFP and 7% for GFP. This probability is based on the approximately 3:1 ratio of recombination between the three common colors and GFP in the Confetti allele (ref. (*16*) and our own unpublished data), and on the observed Mx1-Confetti recombination efficiency of ~90%. For example, recombination efficiency for RFP/CFP (or CFP/RFP) = 2*(0.2*0.2) = 8%.

** Proportions estimated based on the empirical distribution of color combinations across all AID-Confetti-B1-8 GCs from day 3 to day 11 post-tamoxifen, multiplied by 0.4 (the approximate proportion of recombined cells, based on the mean density data for day 7 post-tamoxifen in AID-Confetti mice).

Table S2. Antibodies used for flow cytometry.

Surface molecule	Fluorochrome	Clone	Manufacturer	Final conc. (µg/ml)
B220	BV421	RA3-6B2	Biolegend	0.5
CD16/32 (Fc block)	---	2.4G2	Bio-X-Cell	1.0
CD38	APC	90	Biolegend	0.5
CD45.1	FITC	A20	Biolegend	0.5
FAS	PE-Cy7	Jo2	BD	0.25
IgD	PerCP-e710	11-26C	eBioscience	0.5
IgMa	PE	MA-69	Biolegend	0.5
TCRβ	APC-e780	H57-597	eBioscience	1.0

Online supplementary files

Movie S1

Intravital imaging movie showing a single Z-slice of the cortical region of a popliteal LN from an unimmunized Mx1-Confetti mouse. Cell colors as in fig. S1B. Second-harmonic generation from collagen fibers is in blue. Movie shown at 180X real time.

Movie S2

Intravital imaging movie showing a single Z-slice of the cortical region of a popliteal LN from an Mx1-Confetti mouse 20 days after immunization with CGG. Cell colors as in fig. S1B. Second-harmonic generation from collagen fibers is in blue. A small GC can be visualized in the center of the field as a cluster of larger, slower-moving cells expressing both RFP and membrane CFP. Movie shown at 180X real time.

Movie S3

Intravital imaging movie showing a single Z-slice of the cortical region of a popliteal LN from an Mx1-Confetti mouse 20 days after immunization with CGG. Cell colors as in fig. S1B. Second-harmonic generation from collagen fibers is in blue. A large GC can be visualized in the center of the field as a cluster of larger, slower-moving cells expressing both nuclear GFP and membrane CFP. Movie shown at 180X real time.

Database S1

Sequences of *Igh* and *Igk* genes used to generate phylogenies presented in Figures 4, 5, S9, S10 and sequences of *Igh* genes used to generate clonal distributions in Figures 2, S2, S3. Includes sequence ID (isotype) and anatomical origin; fluorescent protein(s) expressed; *Igh* alignments, junctions and number of mutations according to IMGT and VBASE2; *Igh* nucleotide sequence; and paired *Igk* alignment, junction and sequence.

Additional References

34. L. Madisen *et al.*, A robust and high-throughput Cre reporting and characterization system for the whole mouse brain. *Nature neuroscience* **13**, 133 (Jan, 2010).

35. R. Kuhn, F. Schwenk, M. Aguet, K. Rajewsky, Inducible gene targeting in mice. *Science* **269**, 1427 (Sep 8, 1995).

36. D. Y. Mason, M. Jones, C. C. Goodnow, Development and follicular localization of tolerant B lymphocytes in lysozyme/anti-lysozyme IgM/IgD transgenic mice. *International immunology* **4**, 163 (Feb, 1992).

37. T. A. Shih, M. Roederer, M. C. Nussenzweig, Role of antigen receptor affinity in T cell-independent antibody responses in vivo. *Nat Immunol* **3**, 399 (Apr, 2002).

38. A. G. Schmidt *et al.*, Viral receptor-binding site antibodies with diverse germline origins. *Cell* **161**, 1026 (May 21, 2015).

39. K. Halemano *et al.*, Humoral immunity in the Friend retrovirus infection model. *Immunologic research* **55**, 249 (Mar, 2013).

40. K. K. Dietze *et al.*, Combining regulatory T cell depletion and inhibitory receptor blockade improves reactivation of exhausted virus-specific CD8+ T cells and efficiently reduces chronic retroviral loads. *PLoS pathogens* **9**, e1003798 (2013).

41. E. P. Browne, Toll-like receptor 7 inhibits early acute retroviral infection through rapid lymphocyte responses. *Journal of virology* **87**, 7357 (Jul, 2013).

42. K. Liu *et al.*, In vivo analysis of dendritic cell development and homeostasis. *Science* **324**, 392 (Apr 17, 2009).

43. C. D. Allen, T. Okada, H. L. Tang, J. G. Cyster, Imaging of germinal center selection events during affinity maturation. *Science* **315**, 528 (Jan 26, 2007).

44. Z. Shulman *et al.*, T follicular helper cell dynamics in germinal centers. *Science* **341**, 673 (Aug 9, 2013).

45. J. J. Trombetta *et al.*, Preparation of Single-Cell RNA-Seq Libraries for Next Generation Sequencing. *Curr Protoc Mol Biol* **107**, 4 22 1 (2014).

46. T. Tiller, C. E. Busse, H. Wardemann, Cloning and expression of murine Ig genes from single B cells. *J Immunol Methods* **350**, 183 (Oct 31, 2009).

47. M. P. Lefranc *et al.*, IMGT, the international ImMunoGeneTics information system. *Nucleic acids research* **37**, D1006 (Jan, 2009).

48. I. Retter, H. H. Althaus, R. Munch, W. Muller, VBASE2, an integrative V gene database. *Nucleic acids research* **33**, D671 (Jan 1, 2005).

49. G. Pasqual, A. Angelini, G. D. Victora, Triggering positive selection of germinal center B cells by antigen targeting to DEC-205. *Methods in molecular biology* **1291**, 125 (2015).

50. A. Chao, Nonparametric-Estimation of the Number of Classes in a Population. *Scand J Stat* **11**, 265 (1984).

51. R. K. Colwell *et al.*, Models and estimators linking individual-based and sample-based rarefaction, extrapolation and comparison of assemblages. *J Plant Ecol-Uk* **5**, 3 (Mar, 2012).

52. M. Meyer-Hermann *et al.*, A theory of germinal center B cell selection, division, and exit. *Cell reports* **2**, 162 (Jul 26, 2012).

53. M. Meyer-Hermann, Overcoming the dichotomy of quantity and quality in antibody responses. *Journal of immunology* **193**, 5414 (Dec 1, 2014).

54. H. Gu, D. Tarlinton, W. Muller, K. Rajewsky, I. Forster, Most Peripheral B-Cells in Mice Are Ligand Selected. *Journal of Experimental Medicine* **173**, 1357 (Jun 1, 1991).

55. M. E. Boersch-Supan, S. Agarwal, M. E. White-Scharf, T. Imanishi-Kari, Heavy chain variable region. Multiple gene segments encode anti-4-(hydroxy-3-nitro-phenyl)acetyl idiotypic antibodies. *The Journal of experimental medicine* **161**, 1272 (Jun 1, 1985).